In Situ X-ray Diffraction Study of Crystallization Kinetics in $PbZr_{1-x}Ti_xO_3$ (PZT, x = 0.0, 0.55, 1.0)

Angus P. Wilkinson, James S. Speck, and Anthony K. Cheetham*

Materials Department, University of California, Santa Barbara, California 93106

Srinivasan Natarajan and John Meurig Thomas

Davy Faraday Research Laboratory, The Royal Institution of Great Britain, 21 Albermarle St., London, W1X 4BS, U.K.

Received November 18, 1993. Revised Manuscript Received February 24, 1994®

The crystallization of $PbZr_{1-x}Ti_xO_3$, x = 0 (PT), 0.55 (PZT), and 1.0 (PZ), from alkoxide gels, in air, has been studied by *in situ* by X-ray powder diffractometry at temperatures in the range 380–500 °C. Prior to crystallization, an intermediate fluorite or pyrochlore phase is observed for PZ and PZT but not for PT. This is consistent with zirconium enhancing the likelihood of fluorite phases. The results demonstrate that the crystallization temperatures increase in the sequence PT < PZ < PZT. However, on a homologous temperature scale ($T/T_{melting}$) the crystallization temperature for PT and PZ are both $\sim 0.41 T_{melting}$ and for PZT the crystallization temperature is $\sim 0.46 T_{melting}$. Crystallization at lower temperatures is preceded with an induction period which reflects the time necessary to establish a steady-state population of embryos. The crystallization kinetics were monitored by following the integrated intensity of the $(200)_{cubic}$ perovskite peak with time. Quantitative analysis of the Bragg peak full widths at half-maximum show that the crystallite size saturates to a constant value during crystallization. The value of the saturated particle size increases with increasing crystallization temperature, indicating that the final particle sizes are dictated by nucleation rates. These results are placed in the context of an Avrami analysis of the transformation kinetics.

Introduction

PZT ($PbZr_{1-x}Ti_{1-x}O_3$)-type materials are of commercial interest on account of their excellent piezoelectric, pyroelectric, ferroelectric, and dielectric properties. These characteristics facilitate applications in many areas, including hydrophones, thermal imaging, nonvolatile memories, surface acoustic wave generators, and gas sensors. Their use in integrated ferrocelectric/semiconductor devices,[1,2] such as nonvolatile memories,[3] relies upon the preparation of high-quality thin films of material. Among the many approaches for preparing such films, metal alkoxide precursor routes have proven to be popular and effective (see, for example, Sanchez *et al.*[4]).

Thin films can be prepared from such solutions by spin or dip coating, followed by appropriate heat treatment. The processing conditions required to obtain good-quality materials in the PZT family from such solutions have been investigated by many workers.[5–11] However, most of the effort has been concentrated on lead titanate and PZT solid-solution compositions near to the morphotropic phase boundary due to high dielectric constants, rather than on lead zirconate. Ideally, the ferroelectric pervoskite should be produced at a low temperature in a phase-pure and well-crystallized form. Low processing temperatures ease the fabrication of ferroelectric device elements in the presence of other materials, such as GaAs substrates. In addition, the formation of impurities, such as the pyrochlore $Pb_2(Ti/Zr)_2O_6$, which has apparently been observed by several workers,[5,9,10–12] adversely influence device performance.

The study of kinetic processes, such as crystallization, using diffraction techniques is often carried out using quenched samples. This approach introduces an element of uncertainty into the analysis of the data because quenched samples may not accurately represent the high-temperature situation; for example, there is a distinct possibility of short-lived phases at high temperatures. Additionally, the sample may transform upon quenching. Finally, each time slice requires a different sample, and it is often difficult to reproduce the X-ray diffraction sample packing conditions between experiments, thus introducing an element of uncertainty in quantitative comparisons between time slices. The use of *in situ* diffraction techniques to study dynamic processes eliminates these difficulties but has only recently become a practical option with the advent of better instrumentation and more intense radiation sources. For example, we have

® Abstract published in *Advance ACS Abstracts*, April 1, 1994.

(1) Paz de Araujo, C. A.; Taylor, G. W. *Ferrolectrics* **1991**, *116*, 215.
(2) Scott, J. F.; Paz de Araujo, C. A.; McMillan, L. D.; Yoshimori, H.; Wanatabe, H.; Mihara, T.; Azuma, M.; Ueda, T.; Ueda, T.; Ueda, D.; Kano, G. *Ferrolectrics* **1992**, *133*, 47.
(3) Scott, J. F.; Paz de Araujo, C. A. *Science* **1989**, *246*, 1400.
(4) Sanchez, L.; Dion, D. T.; Wu, S. Y.; Naik, I. K. *Ferroelectrics* **1991**, *116*, 1.
(5) Budd, K. D.; Dey, S. K.; Payne, D. A. Proc. Brit. Ceram. Soc. **1985**, *36*, 107.
(6) Budd, K. D.; Dey, S. K.; Payne, D. A. *Mater. Res. Soc. Symp. Proc.* **1986**, *31*, 711.
(7) Lipeles, R. A.; Coleman, D. J.; Leung, M. S. *Mater. Res. Soc. Symp. Proc.* **1986**, *73*, 665.
(8) Schwartz, R. W.; Lakeman, C. D. E.; Payne, D. A. *Mater. Res. Soc. Symp. Proc.* **1990**, *80*, 335.
(9) Lakeman, C. E.; Payne, D. A. *J. Am. Ceram. Soc.* **1992**, *75*, 3091.
(10) Hirano, S.; Yogo, T.; Kikuta, K.; Araki, Y.; Saitoh, M.; Ogasahara, S. *J. Am. Ceram. Soc.* **1992**, *75*, 2785.
(11) Faure, S. P.; Barboux, P.; Gaucher, P.; Livage, J. *J. Mater. Chem.* **1992**, *2*, 713.
(12) Hirashima, H.; Onishi, E.; Nakagawa, M. *J. Non-Cryst. Solids* **1990**, *121*, 404.

0897-4756/94/2806-0750$04.50/0

been able to monitor the behavior of oxide catalysts during the conversion of natural gas to C_2 hydrocarbons and synthesis gas using both rotating anode X-ray instrumentation[13] and energy-dispersive methods with synchrotron X-rays.[14] In the neutron diffraction area, extensive use has been made of position-sensitive detectors to study a wide range of other reactions.[15-17]

Previous diffraction studies of the crystallization kinetics of ferroelectric materials, for example, PLZT from nitrate solutions,[18] PZMN from a standard ceramic preparaton,[19] and thin PZT films prepared from alkoxides,[20] have used quenched samples. However, there has been an *in situ* study, using Raman spectroscopy, of the formation of $BaTi_5O_{11}$ thin films.[21] Here, we describe an *in situ* study of the crystallization kinetics of three PZT compositions using quantitative high-temperature X-ray diffractometery. The results of these measurements are analyzed using JMAK kinetics[22-26] by fitting to the Avrami equation

$$X = 1 - \exp(-kt^n) \qquad (1)$$

where X is the transformed fraction, t the elapsed time, k a rate constant, and n the order of the reaction. This approach to the treatment of kinetic data has been applied by many workers in a range of fields, including the crystallization of metallic glasses, the modeling of ferroelectric switching phenomena, the processing of sol–gel produced materials,[27-31] the growth of zeolite crystals,[32] polymerization in layered phosphate salts,[33] phase transformations in crystalline materials, and the decomposition of various solid phases.

Experimental Section

Three samples of dried alkoxide-based gel (xerogel) were prepared; one of each of the compositions Pb:Ti 1:1, Pb:Zr 1:1, and Pb:Zr:Ti 1:0.45:0.55 (referred to hereafter as PT, PZ, and PZT, respectively). The starting zirconium/titanium alkoxide solutions were made up by dissolving $Zr(n\text{-}OBu)_4$ (Aldrich)/$Ti(i\text{-}OPr)_4$ (Aldrich) in anhydrous 2-methoxyethanol (Aldrich) to give a metal concentration of about 1.25 M in both cases. The concentrations of the solutions and the lead content of the starting lead acetate trihydrate (Aldrich) were determined gravimetrically.

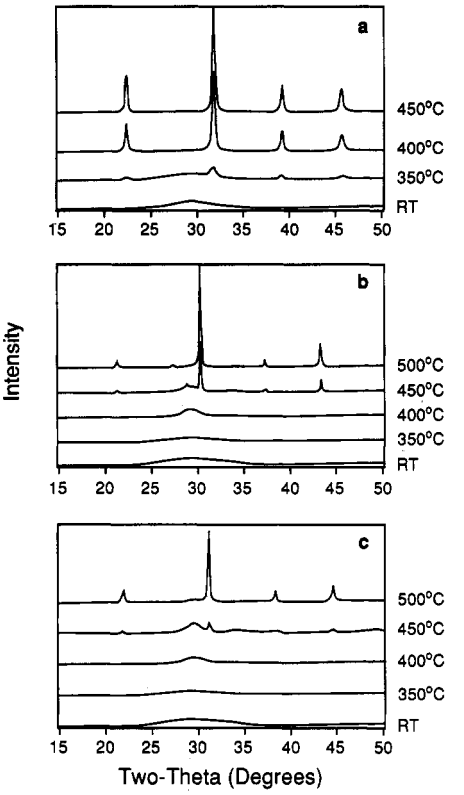

Figure 1. X-ray powder patterns of (a) the PT sample, (b) the PZ sample, and (c) the PZT sample, collected as a function of temperature. The samples were heated at a rate of 10 °C/min between scans, each of which took approximately 20 min.

The lead acetate hydrate (approximately 0.08 mol) was dissolved in about 110 mL of 2-methoxyethanol (Aldrich) and the excess solvent mixture (approximately 80 mL) was removed by distillation. This procedure effectively removes some of the water introduced into the solution with the lead acetate hydrate. The solution was then cooled and stoichiometric amounts of zirconium and/or titanium alkoxide were added from a dropping funnel. Any residue in the funnel was washed into the reaction flask using approximately 25 mL of anhydrous 2-methoxyethanol. The resulting solutions were then briefly refluxed, and excess solvent was once again removed by distillation (about 80 mL). The mixture was allowed to cool to room temperature prior to hydrolysis. These solutions were hydrolyzed by the addition of a water/solvent mix using approximately 3.65 mol of water/mol of alkoxide (15–20 mL of water/solvent mix). The resulting gels were then dried at about 110 °C in a vacuum oven.

X-ray diffraction data were collected as a function of time and temperature on a Siemens D500 diffractometer equipped with a Stöe rotating anode source (Cu target) and a variable-temperature stage.[34] The sample was held, in air, in a pyrophyllite holder, and the temperature was measured with a K-type thermocouple. The dried gels were first heated at temperatures varying between 200 and 300 °C for ~12 h to remove residual volatile materials; without such pretreatment, the gels expanded in the sample holder during X-ray data collection. Data for the three samples ($PbZr_{1-x}Ti_xO_3$, $x = 0, 0.55, 1.0$) were then collected as a function of temperature in the 2θ range ~15–50° for the PZ and PT samples and 15–60° for the PZT sample, with a heating rate of 10 °C/min (Figure 1). In addition, the crystallization kinetics for these samples were studied by following the growth of the $(200)_c$ reflection as a function of time at a series of different temperatures (Figure 2), and the integrated intensities and peak widths (full widths at half-maximum) were obtained by fitting the data to a pseudo-Voigt function (Figure 3).

(13) (a) Jones, R. H.; Ashcroft, A. T.; Waller, D.; Cheetham, A. K.; Thomas, J. M. *Catal. Lett.* **1991**, *8*, 169. (b) Pickering, I. J.; Maddox, P. J.; Thomas, J. M. *Chem. Mater.* **1992**, *4*, 994.
(14) Ashcroft, A. T.; Cheetham, A. K.; Jones, R. H.; Natarajan, S.; Thomas, J. M.; Waller, D. *J. Phys. Chem.* **1993**, *97*, 3355.
(15) Pannetier, J. *Ber. Bunsen-Ges. Phys. Chem.* **1986**, *90*, 638.
(16) Pannetier, J. *Chem. Scr.* **1986**, *26A*, 131.
(17) Damkroger, B. K.; Jensen, D. J.; Edwards, G. R. *Scr. Met.* **1988**, *22*, 287.
(18) Yishikawa, Y.; Tsuzuki, K. *J. Am. Ceram. Soc.* **1990**, *73*, 31.
(19) Chen, S.-Y.; Wang, C.-M.; Cheng, S.-Y. *J. Am. Ceram. Soc.* **1991**, *74*, 2506.
(20) Chen, K. C.; Mackenzie, J. D. *Mater. Res. Soc. Symp. Proc.* **1990**, *80*, 663.
(21) Lu, H.-C.; Schrader, G. L. *Thin Solid Films* **1992**, *220*, 261.
(22) Johnson, W. A.; Mehl, R. F. *Trans. AIME* **1939**, *135*, 416.
(23) Avrami, M. *J. Chem. Phys.* **1939**, *7*, 1103.
(24) Avrami, M. *J. Chem. Phys.* **1940**, *8*, 212.
(25) Avrami, M. *J. Chem. Phys.* **1941**, *9*, 177.
(26) Brown, M. E.; Dollimore, D.; Galeway, A. K. In *Comprehensive Chemical Kinetics*; Bamford, C. H., Tipper, C. F. H., Eds.; Elsevier Scientific: New York, 1980; Vol. 22.
(27) Subbanna, G. N.; Rao, C. N. R. *Eur. J. Solid State Inorg. Chem.* **1989**, *26*, 7.
(28) Wei, W.-C.; Halloran, J. W. *J. Am. Ceram. Soc.* **1988**, *71*, 581.
(29) Li, D. X.; Thomson, W. J. *J. Mater. Res.* **1990**, *5*, 1963.
(30) Lee, J. S.; Yu, S. C. *Mater. Res. Bull.* **1992**, *27*, 405.
(31) Walck, J. C.; Pantano, C. G. *J. Non-Cryst. Solids* **1990**, *124*, 145.
(32) Thompson, R. W. *Zeolites* **1992**, *12*, 680.
(33) Cao, G.; Mallouk, T. E. *J. Solid State Chem.* **1991**, *94*, 59.
(34) Maddox, P. J.; Stachurski, J.; Thomas, J. M. *Catal. Lett.* **1988**, *1*, 191.

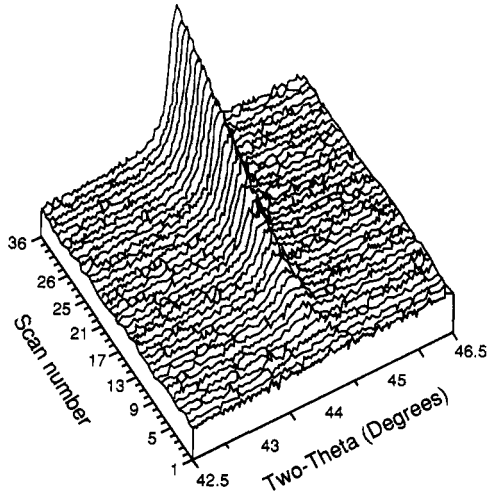

Figure 2. Growth of the intensity of the $(200)_c$ perovskite reflection as a function of time for PZT at 500 °C; each scan took 5 min.

Results and Discussion

Qualitative Results. The variable-temperature measurements on the dried gels (Figure 1) reveal an interesting qualitative result, in that the crystallization of the amorphous material occurs in the temperature sequence $PbTiO_3$ (~390 °C) ≪ $PbZrO_3$ (~480 °C) < $PbZr_{0.4t}Ti_{0.55}O_3$ (~500 °C). These results are similar to findings reported elsewhere.[5,35] Scaling the crystallization temperatures to the melting temperatures of each species ($PbTiO_3$: T_m = 1300 °C; $PbZrO_3$: T_m = 1570 °C; $PbZr_{0.45}Ti_{0.55}O_3$: $T_{liquidus}$ = 1435 °C; $T_{solidus}$ = 1385 °C. $T_{crystallization}/T_{melting}$ = homologous temperature) leads to the homologous temperature sequence $PbZrO_3$ ($0.41T_m$) ≅ $PbTiO_3$ ($0.42T_m$) < $PbZr_{0.45}Ti_{0.55}O_3$ ($0.46(T_{liquidus} + T_{solidus})/2$). Thus for the end members of the PZT system, the transformation kinetics scale very closely with the homologous temperature. Crystallization of the PZT samples may be suppressed due to the enhanced likelihood of compositional fluctuations during the gelation stage of the synthesis. Higher crystallization temperatures may be expected with increasing numbers of components, either due to increased energy necessary for organization or an enhanced likelihood of fluctuations in short-range order. Furthermore, crystallization of PZ probably involves a structural rearrangement in order to accommodate a reduction in the zirconium coordination number from 8 in the dried gel to 6 in the perovskite phase (see below); by contrast, the coordination number of titanium is likely to be octahedral in both cases. The absolute temperatures observed for crystallization for all of the samples appear to be rather lower than those found by other workers. Bud et al.[5] reported crystallization temperatures of about 450, 650, and 550 °C for PT, PZ, and PZT, respectively, in their early work.[5] Subsequently, similar values have been reported by other workers. The lower crystallization temperatures found in the present work may arise from the heating schedule that we employed, in particular the pretreatment in air, or more homogeneous materials during the gelation steps in our synthesis.

The evolution of the diffraction patterns with temperature (Figure 1) also demonstrates that the tendency to form intermediate phases other than the perovskite varies with composition. The PT gel apparently crystallized without the formation of any intermediate phase, while both the PZT and PZ gels form an intermediate phase with wide diffraction maxima (>1° fwhm corresponding to <100-Å particle size). These diffraction maxima can be indexed as the (111) [2θ ~29°], (200) [2θ ~34°], (220) [2θ ~49°], and (311) [2θ ~58°] reflections of a fluorite-type structure. They are usually assigned to a pyrochlore type material related to that observed ($Pb_2Ti_2O_6$) in the crystallization of PbO/TiO_2 containing glasses[37] and hydrothermal preparations of lead titanates. However, there appeared to be no superlattice peaks in our data, leading to the conclusion that the unit cell for this phase is cubic or pseudo-cubic with a ~ 5.25 Å. It seems likely that the intermediate phase is similar in nature to the zirconia/lead oxide fluorite-like solid solution (cubic a = 5.31 Å for 1:1 Pb:Zr) reported by Yamaguchi and coworkers.[37] It is of note that we have only been able to find one paper that presents diffraction data showing the presence of superlattice peaks indicative of a ~10-Å cubic pyrochlore type cell[12] rather than a smaller ~5-Å cubic cell, and even the electron diffraction data for the "pyrochlore" phase reported in Kwok and Desu's[38] study of the pyrochlore to perovskite transition in sol–gel-derived PZT does not show any superlattice peaks. It seems reasonable to us that in zirconium-containing gels the intermediate phase, at least initially, is a fluorite solid solution rather than a well ordered pyrochlore. Since zirconia solid solutions but not those of titania adopt fluorite structures, this would account for the absence of such an intermediate in the PT synthesis.

Pyrochlores,[39] usually formulated as $A_2B_2O_{7-x}$ ($x < 1$), can be described as cation-ordered, anion-vacancy $2a_c \times 2a_c \times 2a_c$ fluorite structures. They contain eight-coordinated A cations and six-coordinated B cations. Oxygen loss ($0 < x < 1$) from such a structure is typically observed with A cations such as lead. Since zirconium has a tendency to adopt coordination numbers higher than 6, for example, in the fluorite-related zirconia structures and, more importantly, in the products of hydrolysis of zirconium/titanium alkoxides,[40] it is likely that the initial xerogel contains zirconium with a coordination number greater than 6. The direct crystallization of this xerogel to a pyrochlore or perovskite structure requires the ordering of the lead and zirconium cations and a reduction in the coordination number of the zirconium, a process that is likely to be sluggish. It appears that the crystallization of a solid solution is able to occur significantly faster than the formation of either of the possible ordered phases.

Further examination of the data shows the presence of a small amount of crystalline PbO (peak at 2θ ~28°, ~1° below the fluorite/pyrochlore peak) in all of the samples. This may be present because of an error in the gravimetric analysis of the starting materials.

Quantitative Results. The increase in the intensity of the $(200)_c$ perovskite peak of the PZT sample at 500 °C is shown in Figures 2. The data for PT at 380 and 400 °C

(35) Chandler, C. D.; Hampden-Smith, M. J. *Chem. Mater.* **1992**, *4*, 1137.
(36) Martin, F. W. *Phys. Chem. Glasses* **1965**, *6*, 143.
(37) Yamaguchi, O.; Fukuoka, T.; Kawakami, Y. *J. Mater. Science Lett.* **1990**, *9*, 958.
(38) Kwok, C. K.; Desu, S. B. *Appl. Phys. Lett.* **1992**, *60*, 1430.
(39) Subramanian, M. A.; Aravamudan, G.; Subba Rao, G. V. *Prog. Solid State Chem.* **1983**, *15*, 55.
(40) Laaziz, I.; Larbot, A.; Julbe, A.; Guizard, C.; Cot, L. *J. Solid State Chem.* **1992**, *98*, 393.

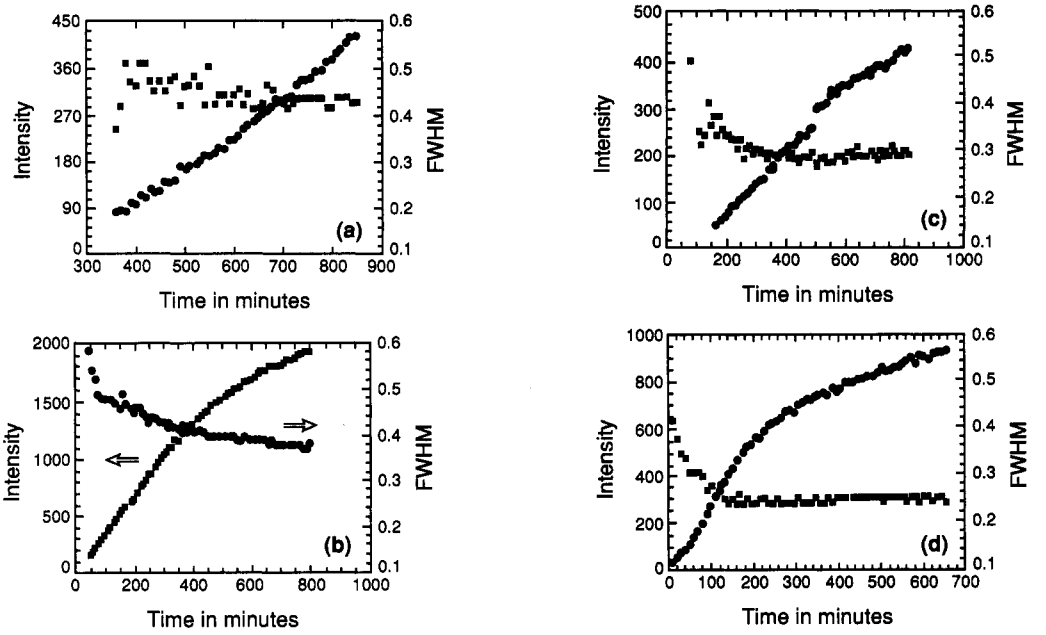

Figure 3. Growth of the integrated intensity of the $(110)_c$ perovskite reflections (left-hand scale) and the decrease in the full width at half-maximum, fwhm in degrees (right-hand scale) as a function of time for (a) PT at 380, (b) PT at 400, (c) PZT at 480, and (d) PZT at 500 °C.

are quantified in parts a and b of Figure 3, respectively, together with the corresponding decrease in the fwhm's as the crystallite size grows. Similar trends are observed in the other systems (e.g. Figure 3c,d). For each sample, the data reveal more rapid crystallization and larger particle sizes at the higher temperature. However, it is found that the particle size obtained from the PZT samples is greater than that from the PT samples, even when the rate of crystallization is broadly comparable (compare parts a and c of Figure 3). This points to a larger number of nuclation points in the PT system. This is consistent with a one-step crystallization in PT directly from amorphous to perovskite (no fluorite phase is observed for the PT crystallization) and a two-step crystallization for PZT via a fluorite phase (which is observed). In the case of PT, there is a high chemical driving force for crystallization and thus a high nuclei density. For PZT, there is again a high driving force for crystallization, but the first phase to appear is fluorite. The crystallization of fluorite reduces the driving force for perovskite crystallization and thus the perovskite nuclei density is lower and the impinging perovskite grain size is larger than for pure PT. A further observation is the pronounced induction period that is observed for both samples at the lower temperatures. This is consistent with sluggish kinetics at lower temperatures. The induction period is recognized to be the time necessary to develop a quasi-steady-state distribution of subcritical embryos.

To quantify the differences between the crystallization processes of the different samples, the rate constants and reaction orders have been determined by fitting the growth of the $(200)_c$ reflection to the Avrami equation. Representative fits are shown in Figure 4, and the rate constants and reaction orders are given in Table 1. It is interesting to note that, in each system, there is a change from a first- to a second-order process as the crystallization temperature is raised. Further, we note that for each case, the fwhm of the Bragg peak saturates to a constant value before the transformation has reached completion. The saturation value of the fwhm decreases with increasing crystallization temperature, corresponding to a larger particle size. The

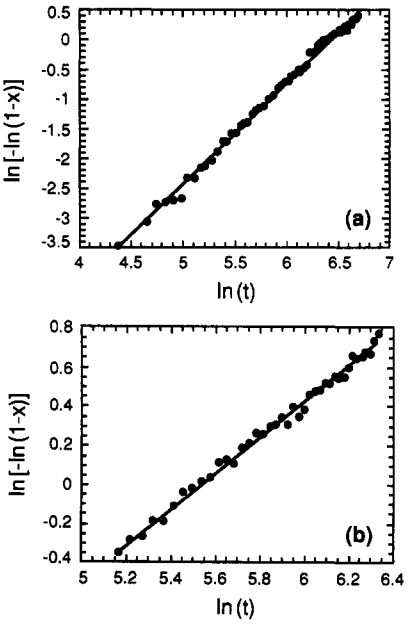

Figure 4. Representative fits of the integrated intensity data for the $(110)_c$ perovskite reflection to the Avrami equation for PZT at (a) 480 and (b) 500 °C.

average particle size calculated by the Scherrer equation is shown in Table 1. The saturation of particle sizes indicates that the crystallized regions grow until impingement with other crystallized regions takes place. There is no evidence for grain growth once crystallization has proceeded to a substantial extent.

For phase transformations in condensed phases, the nucleation rate per unit volume I^V has an approximate temperature dependence given as[41]

$$I^V = c_1 \exp[-c_2/(\Delta T)^2]$$

where c_1 and c_2 are constants characteristic of each system

(41) Christian, J. W. The Theory of Transformations in Metals and Alloys, 2nd ed.; Pergamon: Oxford, 1975.

Table 1. Reaction Orders (n), Rate Constants (k), Saturation $(200)_{cubic}$ Perovskite Peak Width (fwhm), and Saturation Particle Size (d, Calculated from the Scherrer Equation[43]) for the Crystallization of $PbTiO_3$, $PbZrO_3$, and $PbZr_{0.45}Ti_{0.55}O_3$ at Various Temperatures

compound	temp/°C	n	k/s^{-n}	fwhm	d/Å
$PbTiO_3$	380	2.19	3.06×10^{-7}	0.43	199
$PbTiO_3$	390	1.79	7.00×10^{-6}		
$PbTiO_3$	400	1.33	3.71×10^{-4}	0.38	226
$PbZr_{0.45}Ti_{.55}O_3$	480	1.67	2.04×10^{-5}	0.29	296
$PbZr_{0.45}Ti_{.55}O_3$	490	0.99	4.30×10^{-3}		
$PbZr_{0.45}Ti_{.55}O_3$	500	0.90	6.81×10^{-3}	0.25	344
$PbZrO_3$	460	2.06	8.29×10^{-6}	0.13	661
$PbZrO_3$	480	1.03	1.03×10^{-2}		
$PbZrO_3$	490	0.98	2.57×10^{-2}	0.11	750

and ΔT represents the "undercooling" of the amorphous phase; to very good approximation $\Delta T = T_{melting} - T_{crystallization}$. Thus lower crystallization temperatures favor higher nucleation rates. This is consistent with our observation of a smaller particle size, and thus higher nuclei density, with decreasing crystallization temperature. The growth rate reflects thermally activated transport processes across the perovskite/amorphous or perovskite/pyrochlore interface. For the large supercoolings employed in the current crystallization study, the growth rate is expected to follow Arrhenius behavior with a positive activation energy. Thus higher crystallization temperatures promote faster kinetics. Using the concepts of isothermal transformation curves (ITT diagrams),[42] the crystallization temperatures that we have employed fall below the temperatures for maximum transformation rate.

The value of n in the Avrami fits to the transformation data reflects *either* the dimensionality of the transformation or the nature of a diffusion-controlled transformation. It is difficult to differentiate these effects from X-ray diffraction data alone. Values of n in the range 1–2 in the Avrami analysis are consistent with preferred nucleation at surfaces and internal interfaces *or* diffusion-controlled growth.[41] We note, however, that decreasing values of n with increasing crystallization temperature are consistent with selective nucleation at special sites in the powder. TEM analysis on partially transformed powders may clarify the exact nucleation and growth mechanisms.

(42) Reed-Hill, R. E. *Physical Metallurgy Principles*; Van Nostrand: New York, 1973.
(43) Warren, B. E. *X-Ray Diffraction*; Addison-Wesley: Reading, MA, 1969.